Structure and Reactivity of Water Layers on Defect-Free and Defective Anatase TiO_2(101) Surfaces

Antonio Tilocca* and Annabella Selloni

Department of Chemistry, Princeton University, Princeton New Jersey 08544

Received: December 2, 2003; In Final Form: February 11, 2004

The adsorption of thin water overlayers on the (101) surface of TiO_2 anatase has been studied through Car-Parrinello molecular dynamics (CPMD) simulations. We compared the structural and dynamic properties of one and two H_2O monolayers adsorbed on defect-free and partially reduced surfaces at 160 K. As for an isolated adsorbed H_2O molecule, we found that water dissociation is possible only on the defective surface. With respect to a single H_2O, the interaction between H_2O molecules reduces the dissociation barrier: a water molecule incorporated in a monolayer (ML) or a bilayer (BL) over a defected surface dissociates spontaneously at 160 K. On the perfect surface, a water ML forms a regular array of Ti-coordinated molecules, whereas on the defective surface some molecules shift coordination from Ti to a bridging (O_{2c}) oxygen, leading to a mixed ML state with molecular water adsorbed on two different sites and two hydroxyls resulting from the dissociation. Only after adsorption of a second water layer O_{2c}-coordinated molecules are formed also on the regular surface, leading to a more disordered state. Although most structural differences between water overlayers on defect-free and defective surfaces disappear at BL coverage, water molecules are more mobile in the presence of the defect. The presence of H_2O-O_{2c} only above ML coverage and the lack of water dissociation on the defect-free surface are in agreement with the findings of recent temperature-programmed desorption experiments, which have been further analyzed on the basis of the calculated adsorption energies.

1. Introduction

Within the current effort toward a better understanding of water−solid interfaces,[1−4] recently many theoretical investigations have focused on the influence of intermolecular water−water interactions on the structure and reactivity of thin water overlayers on solid surfaces.[5−12] A common important feature emerging from these studies is that water−water interactions act so as to favor the dissociation of adsorbed H_2O molecules, although to a different extent and with different microscopic mechanisms depending on the substrate. Moreover, mixed states where both molecular and dissociated H_2O are present seem to occur with a larger probability with respect to fully dissociated states. Michaelides et al.[9] found that the dissociation of H_2O on Ru(0001) is more favored, both thermodynamically and kinetically, when it is incorporated in a bilayer than when it is isolated. Stirling et al.[10] observed that, although molecular adsorption is always favored, the presence of hydrogen bonds (Hbs) with the second layer H_2O stabilizes dissociated molecules on the (100) surface of pyrite, hindering their recombination to the molecular state. Similarly, an isolated water molecule on undefected MgO(100) does not dissociate, but strong water−water interactions at higher coverage lead to spontaneous dissociation: the molecule accepts an Hb and its intramolecular OH bond is weakened, thus lowering the barrier to proton transfer.[6,7] The formation of multiple Hbs at intermediate coverages facilitates water dissociation also on Al_2O_3(0001), through different mechanisms.[5] On the perfect rutile TiO_2(110) surface, water dissociation becomes favored relative to molecular adsorption only at high coverage,[11] thanks to the formation of hydrogen-bonded hydroxyl chains. Molecular dynamics simulations of multilayer water on the same surface show that a second-layer H_2O may induce a proton transfer from water in the first layer to the surface, as well as multiple proton transfers between water molecules.[12] At the water−silica interface, the participation of a second water molecule in the proton-transfer process removes the barrier to dissociation.[13]

The above remarkable effects on the dissociation probability basically reflect important changes in the surface−water interface which occur when more H_2O molecules are adsorbed. As many applications of TiO_2-based materials involve aqueous solutions,[3] a detailed understanding of the dynamical phenomena occurring in the first water layers is essential. While a clear picture of multilayer water on TiO_2−rutile is starting to emerge,[12] considerably less information is available for the anatase structure, which is more frequently used and more efficient for many photocatalytic applications.[14]

It is well established that for TiO_2 anatase the (101) surface is the most stable one. In a recent TPD study,[15] three water desorption states at 160, 190, and 250 K have been observed, which were attributed to multilayer water, H_2O coordinated to a bridging oxygen (O_{2c}), and H_2O adsorbed on a 5-fold coordinated Ti (Ti_{5c}), respectively. The absence of a high temperature desorption peak characteristic of hydroxyl groups indicates that no dissociated water is present, which has been attributed to the absence of oxygen vacancies on the anatase surface. On the theoretical side, first-principles studies of water on defect-free anatase (101) have shown that molecular adsorption is indeed thermodynamically favored up to ML coverage.[16] In the presence of surface oxygen vacancies, instead, dissociative adsorption leading to the formation of two bridging hydroxyls

* To whom correspondence should be addressed. atilocca@princeton.edu.

10.1021/jp037685k CCC: $27.50
Published on Web 03/20/2004

becomes more favorable in the low coverage limit, with a free energy barrier for dissociation of about 0.1 eV.[17]

To get deeper microscopic insight into the water−anatase interface, in this paper, we present ab initio molecular dynamics simulations of one and two water monolayers adsorbed on both perfect and defective anatase (101) surfaces. The studied systems represent different cases where the complex interactions mentioned above come into play. A direct comparison between their structural and dynamic properties allows us to highlight the main features of the hydrated anatase (101) surface. In particular, our simulations provide new insight into the dynamics of water dissociation at finite coverage as well as a microscopic picture of the different relevant adsorption modes in water overlayers.

2. Computational Method

The calculations have been performed with the Car-Parrinello[18] method as implemented in the CP code.[19] The electron−electron interaction was accounted for by the PBE exchange-correlation functional,[20] whereas ultrasoft pseudopotentials[21] described the ion core−electron interaction. Titanium 3s, 3p, 3d, and 4s shells were included in the valence states. The Kohn−Sham states were expanded in plane waves up to kinetic energy cutoffs of 25 and 200 Ry for the smooth part of the wave function and the augmented density, respectively. The Brillouin zone sampling was limited to the Γ point only. The anatase (101) surface was modeled by four-layer thick periodically repeated slabs, with the atoms of the bottom layer fixed to their equilibrium bulk positions and water adsorbed on the upper surface only. We used the experimental bulk lattice parameters,[22] i.e., $a = 3.782$ Å and $c = 9.502$ Å. A large (1×3) surface cell of 10.24×11.36 Å^2 area was used to model the defective surface in order to effectively separate the defects in adjacent supercells. An oxygen vacancy was created by removing a bridging oxygen from the top layer of the surface, leading to a $Ti_{24}O_{47}$ composition for the supercell. A smaller 1×2 supercell with 10.24×7.57 Å^2 area and $Ti_{16}O_{32}$ composition was used for the simulation of water monolayers on the perfect surface. All these approximations were previously found to be adequate to model TiO_2-water systems.[16,17,23−25] Furthermore, we compared water−water and water−surface radial distribution functions (rdfs) for one adsorbed monolayer calculated with both the 1×2 and 1×3 supercells. Their excellent matching confirms that a 1×2 cell is large enough to capture the main properties of water adsorbed on the perfect surface.

The perfect 1×3 slab used in the simulations is shown in Figure 1. On the perfect anatase (101) surface, rows of fully coordinated (Ti_{6c}) and undercoordinated (Ti_{5c}) Ti atoms running along [010] are connected by 2-fold coordinated (bridging) and 3-fold coordinated oxygen atoms. An adsorbed ML is usually defined as the number of molecules equal to the number of undercoordinated cationic or anionic sites on the perfect surface. In our case, this corresponds to four adsorbed H_2O in the small and six H_2O in the large supercell. Note that the removal of an O_{2c} transforms a Ti_{6c}−Ti_{5c} pair into a Ti_{5c}−Ti_{4c} one. Therefore, six Ti_{5c} and one Ti_{4c} sites are present in our model of the defective supercell. The perpendicular separation between the slabs was ∼10 Å for the ML simulations and was increased to 14.5 Å for simulating bilayer adsorption, to minimize the interaction of topmost H_2O molecules with the upper periodic image of the slab.

A fictitious mass of 700 au and a time step of 0.1 fs, together with the deuterium mass for H atoms, were used to integrate the Car-Parrinello equations of motion. As in our previous work,[17] these rather conservative choices were needed to simulate the defective surface, where the removal of an oxygen leads to a (filled) vacancy state near the bottom of the conduction band and thus to a small energy gap between occupied and empty electronic states.[26] Incidentally, we note that the (Kohn−Sham) energy of this occupied band gap state is 2.8 eV above the bulk valence band edge E_v in our calculations, whereas UPS experiments find it 2.3 eV above E_v.[29] This discrepancy should be attributed to the well-known difficulties of density functional theory in describing single-particle properties.

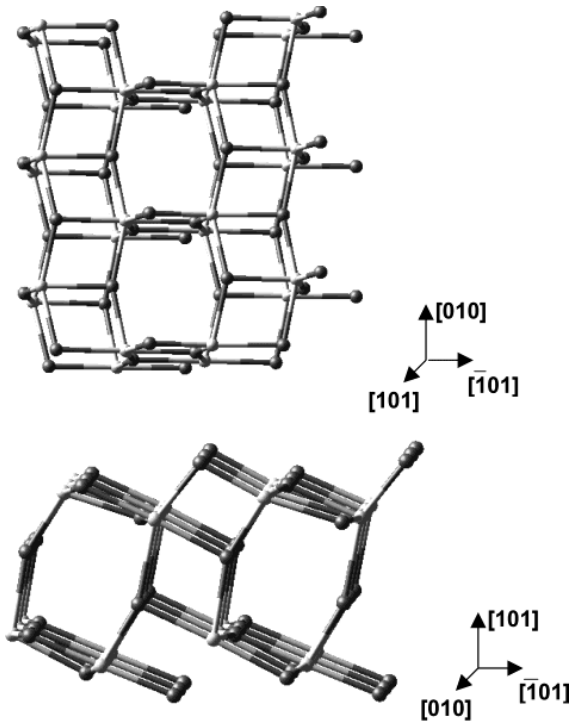

Figure 1. Top and side views of the perfect anatase (101) 1×3 slab used in the calculations. Gray (white) spheres represent O (Ti) atoms.

In the molecular dynamics (MD) trajectories, the ion temperature was kept to an average around 160 K by means of a Nosè thermostat:[27] this is the desorption temperature of multilayer H_2O as measured by TPD experiments.[15] No water desorption was observed in our simulations. Geometry optimizations were carried out by damped dynamics until every component of ionic forces (except on the fixed bottom layer) was below 10^{-3} atomic units. For the defect-free surface, optimized geometries at different water coverages were determined in order to make contact with TPD data. To avoid trapping in local minima, the starting geometries for the structural optimizations were selected among low potential energy configurations generated during the finite temperature simulations. On the defective surface, on the other hand, local optimizations of specific ML structures have been carried out, to evaluate the relative energetics of relevant configurations within an adsorbed ML.

3. Low Coverage Adsorption and Dissociation

We have recently found that several adsorption states exist for an isolated H_2O on the defective anatase (101) surface.[17] Figure 2a shows the geometry of a (nondissociated) molecule adsorbed at the vacancy site, with its oxygen roughly replacing the missing bridging oxygen. Although this structure is rather stable, the molecule moves away from the vacancy at room temperature. The most stable *molecular* adsorption configuration

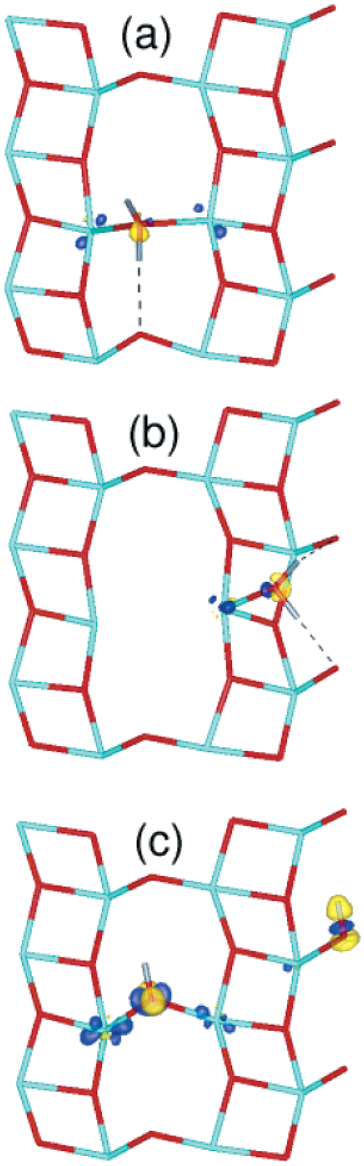

Figure 2. Optimized geometries of one (a,b) intact and (c) dissociated water molecule on the defective anatase(101) surface. Only the top surface layer is displayed; hydrogen bonds are shown as dashed lines. The 0.03 e/a_0^3 isosurface of the charge density difference $\Delta\rho(r)$ is superimposed in each plot. Positive (electron excess) and negative (electron deficit) lobes are shown in yellow and blue, respectively.

is shown in Figure 2b. This molecular state, with both H atoms involved in hydrogen bonds with surface bridging oxygens, is very similar to that occurring on the perfect surface.[16,17] On the defective surface, however, the molecule is adsorbed on a Ti_{4c} rather than on a Ti_{5c}, and thus, its adsorption energy is considerably larger (1.48 vs 0.74 eV). Moreover, on the defective surface, this molecular state is found to be 0.35 eV less stable than the dissociated one shown in Figure 2c. The free energy barrier separating the molecular and dissociated states is about 0.1 eV.[17] Upon dissociation, two bridging hydroxyls (OH_b) are formed, as recently observed for water at oxygen vacancies of the rutile (110) surface.[11,28]

We mentioned in the previous section that the presence of an oxygen vacancy on a TiO_2 surface leads to an occupied band gap state located just below the conduction band minimum,[26] which is associated with the two (reduced) Ti^{3+} ions at the

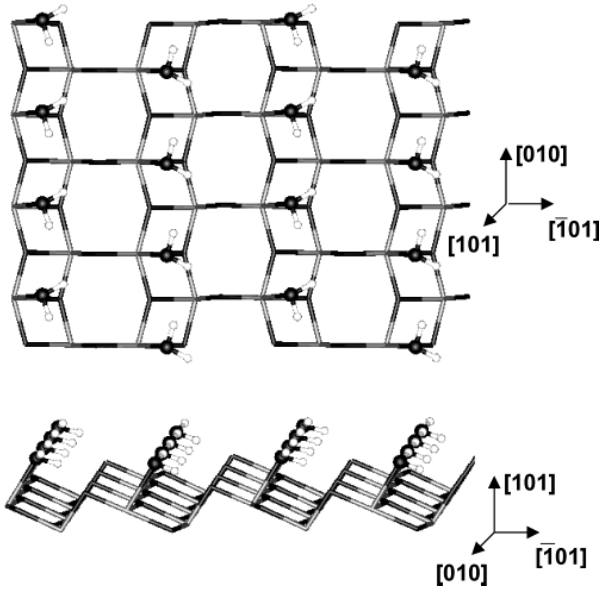

Figure 3. Optimized geometry of a water ML on the perfect surface; top and side views. Water molecules are represented as ball-and-stick; only the surface top layer is shown.

vacancy. Since the hydroxyl is a better electron acceptor than water,[1] a favorable $Ti^{3+} \rightarrow OH^-$ charge transfer interaction (mostly absent when molecular H_2O is adsorbed) could explain the larger H_2O dissociation probability on the defective surface. However, the experimental observation that the band gap state is not affected by water dissociation[30] seems to indicate that only little or no charge transfer from Ti^{3+} to OH^- actually occurs.[26]

To understand the reason of water dissociation on the defective surface, we started by considering the energies of the states in and near the band gap. Consistent with experiment,[30] our results show that the energies of the band gap states for the systems with molecular and dissociated water at the vacancy are very similar. To obtain better insight into the extent of surface/adsorbate charge transfer, we thus examined the density difference $\Delta\rho(\mathbf{r}) = \rho_{H_2O/Anatase}(\mathbf{r}) - \rho_{H_2O}(\mathbf{r}) - \rho_{Anatase}(\mathbf{r})$, where $\rho_{H_2O/Anatase}$ is the density of the interacting water−surface system, whereas ρ_{H_2O} and $\rho_{Anatase}$ are the densities of the two isolated (noninteracting) subsystems, taken in the same geometry of the interacting system. With this definition, the charge flow upon adsorption is from regions where $\Delta\rho(\mathbf{r})$ is negative to regions where it is positive. The comparison of the isodensity contour plots in Figure 2 indicates that the charge transfer from Ti^{3+} to OH^- is definitely more relevant than from Ti^{3+} to molecular H_2O. In particular the shape of lobes in Figure 2c denotes a charge transfer from 3d Ti orbitals to π molecular orbitals of OH^-. On the basis of these results, we conclude that the surface−OH^- charge transfer is likely to have an active role in defect-induced water dissociation.

4. Structure of an Adsorbed Water Monolayer

A starting monolayer configuration was obtained by arranging the H_2O molecules on the undercoordinated surface Ti atoms (four Ti_{5c} atoms for the perfect surface, five Ti_{5c}, and one Ti_{4c} for the defective surface). After a 3 ps equilibration, an MD run of about 4 ps at 160 K was carried out in both cases.

Optimized structures for a water monolayer on the perfect and defective surfaces are shown in Figures 3 and 4. The configuration in Figure 3 represents the optimized, likely the

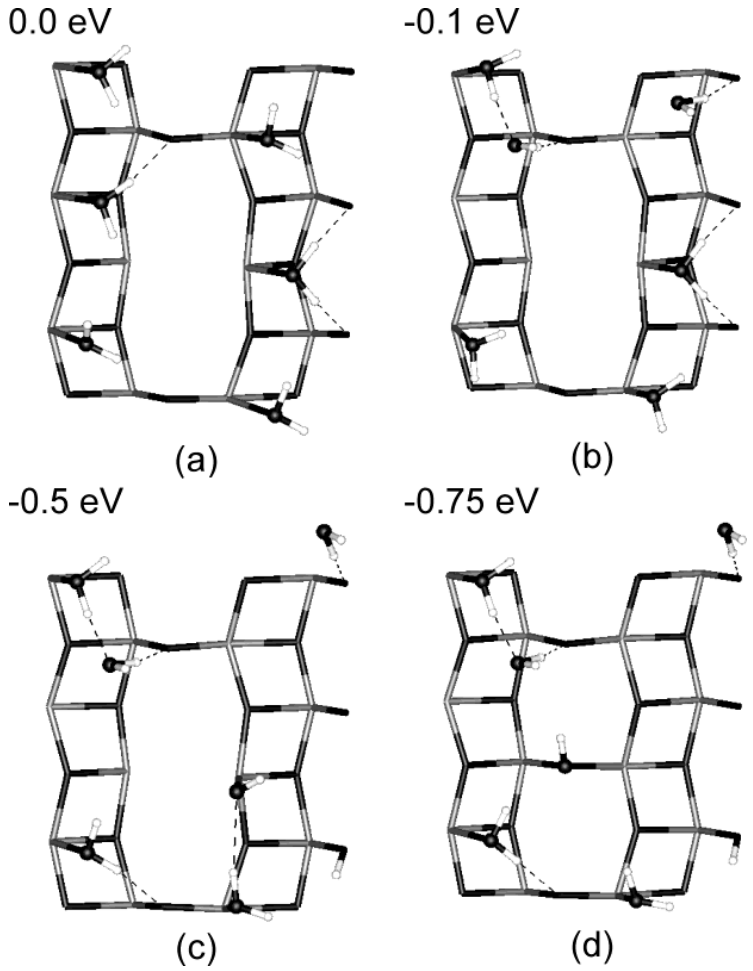

Figure 4. Optimized structures of a water ML on the reduced surface. (a) Six H_2O molecules coordinated to Ti atoms; (b) four (two) H_2O molecules coordinated to Ti (O_{2c}) atoms; (c) same as in b but with a dissociated H_2O, with the hydroxyl in "terminal" coordination; (d) same as in c but with the hydroxyl in "bridging" position. Energies are relative to structure a.

global minimum, structure for a water monolayer on the perfect surface. This was obtained from a starting geometry in which the four molecules had all the same orientation as the single H_2O molecule in Figure 2b (note that this is the same orientation observed for an isolated molecule on the ideal surface[16]). Upon relaxation, the molecules slightly rotate about [101] to form alternate rows in which the molecular dipoles point to different directions, so that the resulting monolayer has a lower net dipole moment with respect to the initial arrangement. The adsorbed molecules are slightly tilted, with the molecular plane forming an angle close to 25° with the surface plane. The adsorption energy per molecule, 0.69 eV, is 0.05 eV smaller than for an isolated H_2O molecule. Essentially, no H_2O-H_2O hydrogen bonds are present, whereas only very weak Hbs link the molecules to the surface.

Figure 4 shows four optimized ML structures, with their relative energies, on the defective surface. These structures represent successive ML configurations during the MD simulation: with six intact water molecules at undercoordinated Ti sites, (a) is the starting geometry which finally evolves to a stable mixed state with two different molecular coordination modes and one dissociated molecule (see below). (c) and (d) differ for the position of the hydroxyl formed by dissociation: terminal in (c), bridging in (d), but are very similar otherwise. At variance with the regular surface, both H_2O-H_2O and H_2O-surface hydrogen bonds are present.

The time evolution of the perpendicular distance of water oxygens (O_w) from the surface, shown in Figure 5, reveals a considerably different behavior of the two surfaces. On the defect-free surface, the water molecules remain very close to their adsorption sites throughout the simulation, giving rise to a single peak centered around 2 Å in the distance distribution (density profile). The overall picture changes substantially on the defective surface: Figure 5b shows that early during the equilibration stage a molecule breaks the $O-Ti_{5c}$ bond, leaving the Ti_{5c} site, and moves ~1 Å above the layer of Ti-coordinated molecules. In this new coordination mode, it forms a strong Hb with an O_{2c}, and its molecular plane is almost perpendicular to the surface, whereas the H_2O-Ti_{5c} molecules form an angle of about 35° with the surface plane. A second $H_2O-Ti_{5c} \rightarrow H_2O-O_{2c}$ shift is observed after additional ~2 ps, leading to the structure shown in Figure 4b, which is 0.1 eV more stable than the initial geometry (Figure 4a). The H_2O-O_{2c} are further stabilized by accepting a Hb from a nearby H_2O-Ti_{5c}, and do not change their coordination any longer in about 5 ps. Two peaks at 2 and 3 Å then arise in the distance distribution of Figure 5b.

The water−water and water−surface rdfs for the ML are reported in Figure 6. On the stoichiometric surface, the structured $g_{O_w-O_w}(r)$ indicates a highly ordered ML in registry with the underlying lattice (Figure 3). Only weak H_2O-O_{2c} hydrogen bonds are present, which give rise to the small

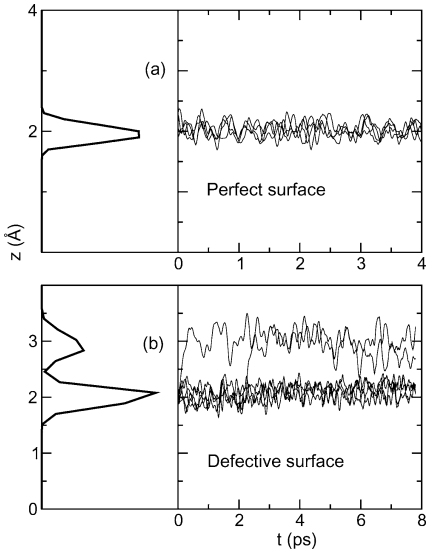

Figure 5. Distribution and time evolution of z (perpendicular distance from the surface) for the water oxygens of an adsorbed ML on (a) perfect and (b) defective surface. z is referred to a Ti atom in the top layer. To show the rearrangements occurring in the water layer on the defective surface, the z evolution during the equilibration has been included in panel b.

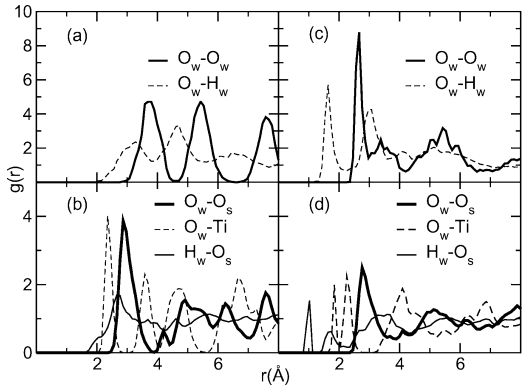

Figure 6. Water−water (top panels) and water−surface (bottom panels) radial distribution functions for an adsorbed ML on the perfect (left) and defective surface (right panels). Subscripts w and s denote water and surface, respectively.

shoulder of $g_{H_w-O_s}(r)$ at 2 Å in Figure 6b. No water−water Hbs are formed: in Figure 6a, the first maxima in $g_{O_w-H_w}(r)$ is at 3.2 Å, whereas that in $g_{O_w-O_w}(r)$ is at 3.8 Å, which corresponds to the distance between neighboring Ti_{5c} sites (as a comparison, the nearest neighbor O−O distance in ice Ih is 2.74−2.77 Å). On the other hand, the rdfs for the ML on the defective surface (structures b−c in Figure 4) show a pattern typical of a H-bonded system. Here, water−water Hbs involve H_2O-O_{2c} as acceptor and H_2O-Ti_{5c} as a donor: these Hbs are evidenced by the first peaks in $g_{O_w-H_w}(r)$ and $g_{O_w-O_w}(r)$, respectively (Figure 6c). The hydrogen bonds linking H_2O-O_{2c} to the surface O_{2c} give rise to a sharp peak at 1.75 Å in $g_{H_w-O_s}(r)$ (mostly missing in the same distribution for the perfect surface) and shift the main peak of $g_{O_w-O_s}(r)$ to 2.77 Å (vs 2.87 Å for the perfect surface).

No water dissociation was observed in the MD simulation for the perfect surface, in agreement with the TPD experiments[15] and with earlier static calculations.[16] On the defective surface, instead, a spontaneous dissociation occurs after 2.3 ps, i.e., soon after the second coordination shift. Not surprisingly, the

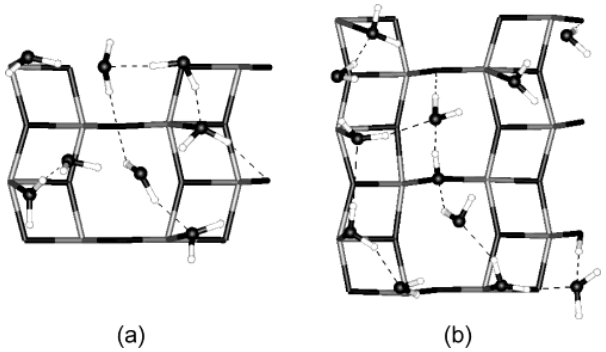

Figure 7. (a) Optimized geometry of an adsorbed water BL on the perfect surface. (b) Snapshot taken from a MD trajectory of a BL on the defective surface. The trajectory was started with the hydroxyl formed by water dissociation located in a bridging position on the vacancy.

dissociation involves the water molecule coordinated to Ti_{4c}, which is the most reactive surface site due to its unusually low coordination. This H_2O-Ti_{4c} transfers a proton along a Hb to a O_{2c}, forming a terminal (OH_t) and a bridging (OH_b) hydroxyl (Figure 4c) with an energy gain of 0.4 eV. The additional short-distance peaks arising from water dissociation are clearly visible in the $g_{H_w-O_s}(r)$ and $g_{O_w-Ti}(r)$ of Figure 6d. The latter peak shows that the Ti−OH bond (r = 1.84 Å) is much stronger than the Ti−OH_2 bond (r = 2.26 Å), as observed also for the water−iron bonds on the pyrite surface.[10] The formation of a shorter Ti−OH bond is not evident in the z trajectory of Figure 5b, where only the z component of the Ti−O distance is considered. In fact, Figure 4c shows that the Ti−OH bond is roughly perpendicular to the surface (thus $\Delta z \sim R_{Ti-OH} \sim 1.9$ Å), whereas the Ti−OH_2 bonds are significantly tilted (thus $R_{Ti-OH_2} > \Delta z \sim 2$ Å), so that the corresponding $z(t)$ trajectories overlap.

After the H_2O dissociation on the defective surface, we did not observe OH_t moving to the vacancy to form a bridging hydroxyl; instead, it remained in the intermediate position shown in Figure 4c, where it can accept a Hb from the neighboring H_2O-Ti_{5c}. However, similarly to what we previously found for a single adsorbed H_2O,[17] the ML structure with the hydroxyl in bridging position (Figure 4d) is 0.25 eV more stable than the structure with the terminal hydroxyl in Figure 4c, so that it most likely represents the final, stable state for a dissociated ML on the defective surface.

5. Structure of an Adsorbed Water Bilayer

A second layer of water molecules was added to a configuration extracted from the ML dynamics, and after a 2 ps equilibration run, a 160 K trajectory of ~6 ps was calculated for both the perfect and defective surfaces. Representative BL structures on both surfaces are shown in Figure 7, whereas the time evolutions (with corresponding distributions) of the water oxygen vertical distances from the surface are shown in Figure 8.

On the stoichiometric surface, during the equilibration stage, two H_2O of the second layer move closer to the surface, forming Hbs with the bridging oxygens, as shown in Figure 7a. This H_2O-O_{2c} coordination mode is similar to the one found for the ML on the defective surface (Figure 4b−d), even though their orientation is different: H_2O-O_{2c} molecules in the BL have both hydrogens pointing toward the surface, while one hydrogen is pointing upward in the case of H_2O-O_{2c} incorporated in a ML. Figure 8a shows that the H_2O-O_{2c} molecules occupy an intermediate position between the first layer (located

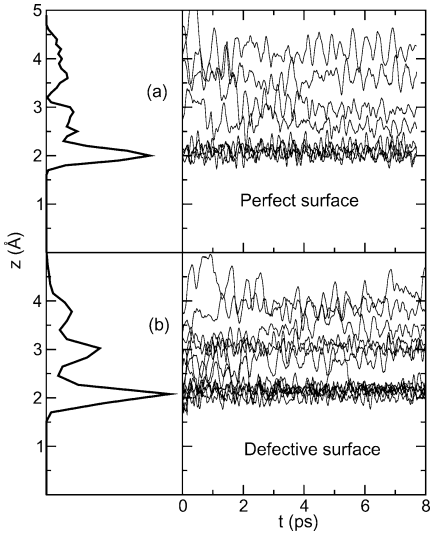

Figure 8. Distribution and time evolution of z for the water oxygens of an adsorbed bilayer on (a) the perfect and (b) the defective surface.

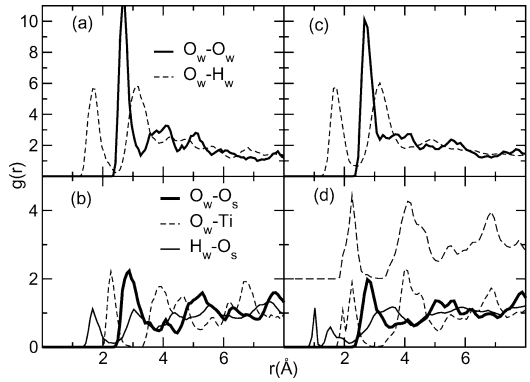

Figure 9. Water−water and water−surface radial distribution functions for a water BL on the defect-free (left panels) and defective (right panels) surfaces. In panel d, the additional O_w−Ti rdf calculated from the run with both hydroxyls in bridging position is shifted vertically for clarity.

about 2 Å above the surface) and the second layer H_2O molecules (molecules located between 3.5 and 4.5 Å above the surface), forming H bonds with both H_2O−Ti_{5c} and the second-layer H_2O. From Figure 8a, it also appears that the two H_2O−O_{2c} are at different distances from the surface, and the same is true for the two H_2O in the second layer, resulting in two broad peaks in the distance distribution after the first layer peak.

On the defective surface, the layering is more pronounced: three distinct peaks arise in the distribution of H_2O−surface distances (Figure 8b), corresponding to H_2O−Ti_{5c} (molecules with 1.5 Å < z < 2.5 Å), H_2O−O_{2c} (molecules with 2.5 Å < z < 3.5 Å), and second layer H_2O (molecules with 3.5 Å < z < 4.5 Å). The first two peaks match the corresponding ones for the ML on the same surface. The relative number densities of the three peaks are 3:2:1.

At variance with what is observed for a ML, the main structural features of an adsorbed BL on the perfect and defective surface are very similar. The water−water rdfs (Figure 9a) on the defect-free surface show now a hydrogen-bonded pattern (as opposed to the curves in Figure 6a), whereas the formation of Hbs with the surface is highlighted by the first peak in $g_{H_w-O_s}(r)$ of Figure 9b. These new features are evident in the BL structure shown in Figure 7a. The H_2O−H_2O rdfs

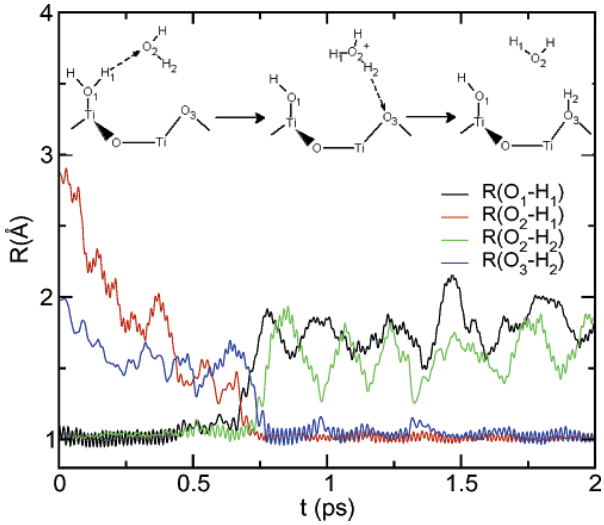

Figure 10. H_2O BL on the defective surface: time evolution of representative distances between atoms involved in the dissociation process. Labels are defined in the inset.

show little difference on the two surfaces (the additional peaks at short distances in $g_{H_w-O_s}(r)$ and $g_{O_w-Ti}(r)$ on the defective surface arise from water dissociation, see below). Comparing the position of peaks corresponding to H_2O-surface Hb in Figure 9, parts b and d, one may infer that H_2O−surface Hbs are slightly stronger on the defective surface.

As for the ML case, also at BL coverage, no dissociation is observed on the perfect surface, whereas dissociation takes place on the defective surface. In the latter case, however, the mechanism of the dissociation is different from the ML case. The dissociation mechanism is sketched in the inset of Figure 10, which reports the time evolution of selected interatomic distances in the first 2 ps of the trajectory. After 0.7 ps, the water molecule chemisorbed on the Ti_{4c} site transfers a proton to a second layer molecule to form a hydronium ion. This transient species lasts only for ∼50 fs and then donates a proton to a surface O_{2c}. The entire process is completed in ∼0.2 ps, and the resulting species are again an OH_t and an OH_b. As for the ML case, the OH_t formed by dissociation does not migrate to the vacancy. The OH_t tends to accept Hbs mainly from second layer water molecules while its proton is not often involved in Hbs.

To study the influence of terminal vs bridging hydroxyls on the structure of the BL, we run another 4 ps MD trajectory, starting from a bilayer configuration with a dissociated water forming two bridging hydroxyls, and no terminal hydroxyl (as in Figures 2c and 4d). The bridging hydroxyl remained in the vacancy site during the whole trajectory, with its proton frequently H-bonded to a H_2O−O_{2c} and accepting another Hb from a second layer H_2O, as shown in Figure 7b. No relevant differences in the BL structure are induced by this coordination, so that the main features discussed above are not affected. The only change in the rdfs occurs in the short distance peak of the Ti−O_w rdf of Figure 9d. In the corresponding rdf calculated from the last trajectory (superimposed in Figure 9d), only a small shoulder is left, indicating that the Ti_{4c}−OH bond is weakened when the hydroxyl is shared with a Ti_{5c}.

6. Discussion

6.1. Water Dissociation. In agreement with theoretical predictions[16] and TPD data,[15] no water dissociation took place

at any coverage on the perfect surface in our MD simulations. Not only are oxygen vacancies a necessary requirement for the dissociation to occur but water dissociation is spontaneous at ML and BL coverage on the defective surface. We previously calculated a free energy barrier of 0.1 eV for the water-defective surface proton transfer at low coverage,[17] and no dissociation was observed in a 6 ps MD at room temperature. The fact that the same process occurs spontaneously (on the same time scale) at 160 K when the molecule is incorporated in a ML or BL on the defective surface indicates that water−water interactions have an active role in lowering the energy barrier for dissociation. This lowering cannot be attributed to the fact that both H_2O hydrogens are donated in Hbs to the surface in the time prior to the dissociation, because the same was true for the isolated H_2O (see Figure 2a). Accepting a hydrogen bond from a second water molecule can weaken the intramolecular OH bond,[7] but a direct inspection of both ML and BL trajectories shows that the dissociated molecule does not accept Hbs from neighboring H_2O molecules before dissociating. In both ML and BL trajectories, however, we find that immediately after the proton transfer the OH_t accepts a Hb from another H_2O, suggesting that the lowering of the dissociation barrier may be due to stabilization of both the transition and product states. This stabilization may be quantified: the structure shown in Figure 4c is 0.4 eV more stable than the undissociated one in Figure 4b. It is interesting to remark that, at low coverage, the dissociation step is thermoneutral, because no stabilization of the terminal hydroxyl through Hbs is present.[17] The driving force of the dissociation at low coverage is the following migration of the hydroxyl to the bridging position, reflecting the low stability of isolated OH_t on TiO_2 surfaces.[28,31] The stabilization of the terminal hydroxyl by hydrogen bonds may explain why no spontaneous migration to the bridging position was observed in the ML and BL simulations: the energy gain resulting from this migration (Figure 4d) is lower (0.25 eV vs 0.37 eV[17]) than at low coverage. Moreover, the migration of OH_t at low coverage was spontaneous at room temperature, but a low barrier (possibly connected to the Hb links) may be present and hinder the migration process at 160 K. Since our calculations show that ML and BL structures with a bridging hydroxyl in the vacancy are energetically favored, it is likely that the migration of OH_t to occupy the vacancy does occur also at high water coverages, but on longer time scales. In other words, the final state of the dissociation should involve only bridging hydroxyls, like in Figures 4d and 7b.

The water dissociation pathway on the defective surface is influenced by the coverage. A direct proton transfer from a molecule coordinated to Ti_{4c} is observed at low[17] and ML coverage. For the BL, instead, an indirect transfer is observed, where two molecules are involved and the exchanged protons move along strongly directional Hb links connecting them. This concerted proton transfer mediated by a second water molecule has been previously observed for water at intermediate coverage on Al_2O_3,[5] for water adsorbed above a ML on the rutile (110) surface,[12] and on a silica surface.[13] Moreover, the recombination to molecular water described by Stirling et al.[10] in the presence of second layer H_2O is exactly the reverse of the indirect dissociative process we observed. Larger coverages are thus likely to further increase the dissociation probability close to a surface vacancy, by providing additional reaction paths through which the dissociation can proceed.

6.2. Layer Structure vs Coverage. Structural and dynamical changes in water layers with increasing coverage appear to be closely related to changes in the hydrogen bond network linking water molecules to each other and to the surface. The interpretation of these modifications can be simplified through a direct hydrogen bond analysis. Using a geometrical definition of Hbs,[32] we calculated the average number of hydrogen bonds per water molecule and their properties over each MD trajectory. The results are shown in Table 1.

TABLE 1: Water−Water and Water−Surface Hydrogen Bond Statistics, Averaged over the MD Trajectories[a]

	perfect surface		defective surface	
	ML	BL	ML	BL
		H_2O-H_2O		
$\bar{n}_{HB}$	0.03	2.11	0.85	2.13
$\bar{R}_{O_w-O_w}$	3.22	2.76	2.75	2.80
$\bar{R}_{O_w-H_w}$	2.30	1.78	1.73	1.80
$\bar{\tau}$	50	311	126	259
		$H_2O-Surface$		
$\bar{n}^*_{HB}$	0.61	1.02	0.58	1.15
$\bar{n}_{HB}$	0.61	0.51	0.58	0.48
$\bar{R}_{O_w-O_s}$	3.04	2.87	2.81	2.76
$\bar{R}_{O_s-H_w}$	2.11	1.91	1.81	1.77
$\bar{\tau}$	157	192	229	379

[a] $\bar{n}_{HB}$: number of Hbs per H_2O molecule; $\bar{R}_{O_w-O_w}$, $\bar{R}_{O_w-H_w}$: average intermolecular distances (Å) of water molecules linked by a Hb; $\bar{\tau}$: mean lifetime (fs) of a Hb. In the case of water−surface Hbs, the average number of hydrogen bonds per surface O_{2c} site ($\bar{n}^*_{HB}$) is also reported.

For adsorption of a water ML, an ordered molecular arrangement was found to be stable on the perfect surface. However Table 1 shows that essentially no Hbs connect water molecules on the perfect surface. This is a consequence of the large distance (∼3.8 Å) between the Ti_{5c} adsorption sites. The complete lack of a hydrogen bond network between H_2O molecules distinguishes this ordered, solidlike water layer from icelike layers, which have sometimes been reported to form when water is adsorbed on solid surfaces.[33−35]

On the defective surface, the presence of an oxygen defect induces important changes in the coordination mode of ML water, with the formation of H_2O molecules directly coordinated to O_{2c}. Since H_2O-O_{2c} are formed from H_2O-Ti_{5c}, the coordination of surface Ti_{5c} is not complete for a ML on the defective surface. The structure with two H_2O-O_{2c} (Figure 4b) on the defective surface is 0.1 eV more stable than the structure with every water molecule coordinated to a Ti atom (Figure 4a). The reason an ordered ML, although very stable on the perfect surface, is destabilized in the presence of a vacancy deserves further comments. The loss of H_2O-Ti_{5c} coordination is not induced by the formation of the hydroxyl, as the two $H_2O-Ti_{5c} \rightarrow H_2O-O_{2c}$ shifts occur before the dissociation. Although the H_2O-O_{2c} coordination is highly stabilized by the presence of H_2O molecules on adjacent Ti_{5c} atoms (see next section), this effect is present also on the ideal surface, so that it cannot explain the shift of coordination on the defective surface. The destabilization of an ordered ML on the defective surface is likely related to a large surface stress induced by the vacancy, which is released by breaking two adjacent H_2O-Ti_{5c} bonds. The release of this stress, together with the formation of H_2O-O_{2c} Hbs, largely balance the loss of H_2O-Ti_{5c} coordination. The same $H_2O-Ti_{5c} \rightarrow H_2O-O_{2c}$ shifts are not possible in the case of a BL adsorbed on the defective surface because in that case the H_2O molecules in the second layer tend to occupy the O_{2c} sites (Figure 7b).

Table 1 shows that on the defective surface almost every molecule in the ML is involved in a strong Hb with another H_2O molecule: these Hbs are generally donated from a H_2O-

Ti_{5c} to a H_2O-O_{2c}, as shown in Figure 4b−d: note that if PBCs are taken into account, the top-right molecule accepts another Hb from the molecule in the bottom-right. Although the number of H_2O−surface Hbs per O_{2c} site are about the same on the perfect and reduced surfaces, the corresponding average R_{OO} and R_{OH} intermolecular distances as well as the Hb mean lifetimes are different, revealing the different Hb strengths, which in turn depends on their different nature. On the perfect surface, the (weak) proton donors are H_2O-Ti_{5c}, whereas on the defective surface, the proton is donated to O_{2c} by water molecules not coordinated to Ti_{5c} (Figure 4b−d).

After adsorption of a second layer of water molecules, the structure of adsorbed H_2O on the perfect surface is modified, as the solidlike structure is lost in favor of a less ordered arrangement. A comparison of Figures 3 and 7a shows that the first water layer is significantly perturbed: the H_2O molecules remain in registry with the Ti_{5c} sites, but their orientation is less symmetrical and their plane is more tilted with respect to the ML. The arrangement of the other H_2O molecules is even less ordered: two molecules are close to the surface, coordinated to O_{2c}, and only two H_2O are left in the top layer. H_2O-O_{2c} coordination pairs are similar to the ones found on the defective surface already at ML coverage; at variance with the latter case, H_2O-O_{2c} can now be formed without involving H_2O-Ti_{5c}, so that their formation does not directly involve the first layer. There is an indirect effect, however, as the incorporation of first layer H_2O in an extended network of Hbs with the other molecules leads to the distortion described above. Table 1 shows a net increase in number and strength of both H_2O-H_2O and H_2O−surface Hbs in the BL compared to the ML. On average, every molecule is linked to two H_2O, and every surface O_{2c} accepts a Hb from a H_2O; however, the latter Hbs come both from H_2O-Ti_{5c} and H_2O-O_{2c}, and actually not all of the O_{2c} sites are occupied by H_2O-O_{2c} at this coverage.

The structure of BL on the defective surface in Figure 7b is rather similar to the BL arrangement on the regular surface. The first water layer is complete in both cases, with the molecules tilted more or less to the same extent (∼45°). H_2O-O_{2c} coexist with H_2O-Ti_{5c}, and all H_2O molecules partake of an extended Hb network. The presence of the vacancy leads to slightly weaker H_2O-H_2O Hbs and stronger Hbs linking H_2O to the defective surface. These results show that the presence of an oxygen defect considerably influence the local structure of adsorbed water at ML coverage, but differences are leveled off at BL coverage.

To obtain an estimate of the mobility of adsorbed H_2O we calculated the variance of oxygen atoms positions (mean square displacements), reported in Table 2. For comparison, the corresponding value for ice Ih determined by neutron diffraction[36] ranges from 0.045 $Å^2$ at 123 K to 0.09 $Å^2$ at 223 K. From Table 2, it appears that H_2O molecules adsorbed on anatase-(101) move mainly parallel to the surface. The first layer becomes less mobile when the second layer is adsorbed: at BL coverage, first layer H_2O molecules are less mobile wrt. H_2O in ice. The mobility increases with the distance from the surface, going beyond the ice range for second layer H_2O. The low mobility of the first layer is not affected by the presence of the vacancy, since it is mostly determined by the strong bond to the Ti atoms. On the other hand, H_2O-O_{2c} and second-layer H_2O are definitely more mobile on the defective surface. Therefore, although with the adsorption of a second layer the structural differences observed at ML coverage are much less marked, differences in the dynamic behavior are still present.

TABLE 2: Total Mean Square Displacement (σ^2) and Components Parallel ($\sigma^2_{\parallel}$) and normal ($\sigma^2_{\perp}$) to the Plane of the Surface for Adsorbed Water Molecules, in Å²

	σ^2	$\sigma^2_{\parallel}$	$\sigma^2_{\perp}$
	ML		
H_2O-Ti_{5c}	0.079	0.066	0.013
	ML/def		
H_2O-Ti_{5c}	0.078	0.068	0.010
H_2O-O_{2c}	0.196	0.159	0.037
	BL		
H_2O-Ti_{5c}	0.049	0.038	0.011
H_2O-O_{2c}	0.061	0.050	0.011
second layer H_2O	0.147	0.112	0.035
	BL/def		
H_2O-Ti_{5c}	0.046	0.038	0.008
H_2O-O_{2c}	0.192	0.177	0.015
second-layer H_2O	0.255	0.218	0.037

7. Discussion of Experimental Data

To make contact with recent TPD data,[15] we calculated the adsorption energy of a water molecule at various coverages on the perfect surface. For N adsorbed molecules, we define the average adsorption energy per molecule as $\Delta H_{ads} = -[E_{tot} - E_{bare} - N \cdot E_{wat}]/N$, where $E_{tot}(E_{bare})$ are the energy of the slab with (without) adsorbate and E_{wat} is the energy of a gas-phase water molecule (calculated in the same supercell used for the surface studies). In this way, we obtain $\Delta H_{ads} = 0.74$ eV for water at Ti_{5c} sites of the defect-free surface in the low coverage (0.25 ML) limit, and a smaller value, $\Delta H_{ads} = 0.69$ eV, for ML coverage. A Redhead analysis[37] with a preexponential factor of 10^{13} yields $T_{des} = 268$ and 250 K as the corresponding desorption temperatures. This is in very good agreement with the TPD experiment,[15] where the center of the broad peak corresponding to water adsorbed on Ti_{5c} shifts on roughly the same range of temperatures by increasing coverage until the ML is completed.

For water coverages higher than one ML, a second peak at 190 K is observed in the experimental spectrum, which saturates at BL coverage. This peak was assigned to water adsorbed to O_{2c}, whereas a third peak at 160 K was assigned to the desorption of multilayer (>2 ML) water. For the adsorption energy of an isolated H_2O adsorbed to a O_{2c}, however, we find $\Delta H_{ads} = 0.34$ eV, which corresponds to $T_{des} = 126$ K. Such a low value of the desorption temperature suggests that H_2O-O_{2c} must be stabilized by neighboring H_2O adsorbed to Ti_{5c}. In fact, after adding a second H_2O on a nearby Ti_{5c} and reoptimizing, ΔH_{ads} increases to 0.69 eV per molecule. Taking into account the adsorption energy for an isolated H_2O-Ti_{5c}, this yields 0.635 eV as adsorption energy for H_2O-O_{2c} coadsorbed with a H_2O-Ti_{5c}. This value gives a qualitative insight of the stabilization of H_2O-O_{2c} by coadsorbed water, but it is not clear whether this provides a realistic estimate of the desorption temperature, because desorption of H_2O-O_{2c} likely occurs when all of the surface Ti_{5c} are still occupied and additional H_2O-O_{2c} are present. We thus decided to estimate the desorption temperature by the following procedure. A structure with four H_2O-Ti_{5c} and two H_2O-O_{2c} (corresponding to 1.5 ML), obtained by removing the two second layer molecules from the BL structure in Figure 7a, was allowed to relax by running a short MD trajectory. Five low energy configurations were selected from the trajectory; for each of them, we calculated the adsorption energy as ΔH_{ads} (H_2O-O_{2c}) $= -[E_{1.5ML} - E_{1.5ML-1} - E_{wat}]$, where $E_{1.5ML}$ and $E_{1.5ML-1}$ are the energies of the structure optimized with and without a H_2O-O_{2c}, respectively. The ΔH_{ads} (H_2O-O_{2c}) averaged over the five optimized

configurations is 0.54 ± 0.06 eV, yielding T_{des} = 176÷219 K. This estimated range for H_2O-O_{2c} desorption fits nicely the TPD peak so that the desorption of H_2O-O_{2c} from a 1.5 ML structure seems a sound assumption. Moreover, all our simulations clearly show that on the perfect surface no H_2O-O_{2c} are formed before completing ML coverage, in agreement with the experimental observation that the H_2O-O_{2c} desorption peak is formed after saturation of the ML peak.

The same procedure described above was repeated to estimate the adsorption energy of a second layer water molecule, by optimizing five configurations extracted from the BL dynamics, with and without a second layer H_2O. In this way, we obtained ΔH_{ads} (second layer H_2O) = 0.61 ± 0.03. Although this value is larger than ΔH_{ads} (H_2O-O_{2c}), they overlap if error bars are taken into account, so that it is likely that both H_2O-O_{2c} and second-layer H_2O contribute to the 190 K peak in the TPD spectrum. This was confirmed by another approach to the estimation of desorption temperatures, directly involving the optimized ML, 1.5 ML, and BL as initial and final adsorption states. We considered the following processes: (i) ML-anatase + 2 H_2O → 1.5 ML-anatase, (ii) 1.5ML-anatase + 2H_2O → BL-anatase, and (iii) ML-anatase + 4H_2O → BL-anatase. The adsorption energy per molecule for process A + $N H_2O$ → B was calculated as $-[E(B) - E(A) - N \cdot E_{wat}]/N$. Processes i−iii all lead to similar adsorption energies around 0.65 eV/molecule, confirming that the adsorption/desorption of H_2O-O_{2c} and second-layer H_2O have the same energetics. As discussed in section 6.2, only half of the O_{2c} sites are occupied at BL coverage: H_2O above the first layer are evenly distributed among H_2O-O_{2c} and second-layer, and their desorption is equally likely.

It should be remarked that, besides the intrinsic difficulty in defining reliable initial and final states for the desorption, our approaches do not consider the kinetic nature of the desorption process. A more accurate match to the TPD spectrum would probably require the inclusion of these effects.

8. Summary and Conclusions

In this work, we have presented an ab initio molecular dynamics study of multilayer water adsorption on the (101) surface of TiO_2 anatase, likely the most widely used material in photocatalysis. We have analyzed how the structure of the adsorbed water overlayer changes going from a single monolayer to a bilayer, and also compared the cases of defect-free and defective (partially reduced) surfaces. As for the rutile (110) surface, we found that water dissociation occurs only in the presence of surface oxygen vacancies, and this is likely driven by a charge transfer from the reduced Ti^{3+} near the vacancy to OH^-. A water molecule incorporated in a ML or a BL on the defective surface dissociates spontaneously at 160 K, whereas on the same time scale, no dissociation was observed at room temperature for an isolated H_2O. This suggests that H_2O-H_2O interactions favor the dissociation, by stabilizing the intermediate and/or product states; a 0.4 eV stabilization of the dissociated state is indeed found for a monolayer an the defective surface. Moreover, at larger coverage, additional dissociation paths become available.

We have also shown that oxygen vacancies strongly affect the structure of a water monolayer, whereas their influence is already much weaker for the case of a bilayer. Finally, our results allow us to provide a detailed analysis of recent TPD measurements for the H_2O−anatase(101) system. In particular, we describe the shift of the high-temperature peak with coverage and show that the intermediate temperature peak arises from both H_2O molecules coordinated to the O_{2c} sites and second layer molecules lying slightly above these sites.

Acknowledgment. This work was supported by the National Science Foundation (Grant No. CHE-0121432). The calculations were performed on the Lemieux Terascale Computing System at PSC, Pittsburgh, the IBM SP3 at the Keck Materials Science Computing Center in Princeton, and the Cadillac cluster at the Princeton Institute for Computational Science and Engineering.

References and Notes

(1) Thiel, P. A.; Madey, T. E. *Surf. Sci. Rep.* **1987**, *211*, 385.
(2) Henderson, M. A. *Surf. Sci. Rep.* **2002**, *46*, 1.
(3) Brown, G. E., Jr.; et al. *Chem. Rev.* **1999**, *99*, 77.
(4) Menzel, D. *Science* **2002**, *295*, 58.
(5) Haas, K.; Schneider, W. F.; Curioni, A.; Andreoni, W. *Science* **1998**, *282*, 265.
(6) Giordano, L.; Goniakowski, J.; Suzanne, J. *Phys. Rev. Lett.* **1998**, *81*, 1271−1273.
(7) Odelius, M. *Phys. Rev. Lett.* **1999**, *82*, 3919−3922.
(8) Feibelman, P. J. *Science* **2002**, *295*, 99.
(9) Michaelides, A.; Alavi, A.; King, D. A. *J. Am. Chem. Soc.* **2003**, *125*, 2746−2755.
(10) Stirling, A.; Bernasconi, M.; Parrinello, M. *J. Chem. Phys.* **2003**, *118*, 8917−8926.
(11) Schaub, R.; Thostrup, P.; Laegsgaard, E.; Stensgaard, I.; Norskov, J. K.; Besenbacher, F. *Phys. Rev. Lett.* **2001**, *87*, 266104.
(12) Zhang, C.; Lindan, P. J. D. *J. Chem. Phys.* **2003**, *118*, 4620−4630.
(13) Du, M.-H.; Kolchin, A.; Cheng, H.-P. *J. Chem. Phys.* **2003**, *119*, 6418−6422.
(14) Kavan, L.; Grätzel, M.; Gilbert, S. E.; Klemenz, C.; Scheel, H. J. *J. Am. Chem. Soc.* **1996**, *118*, 6716.
(15) Herman, G. S.; Dohnàlek, Z.; Ruzycki, N.; Diebold, U. *J. Phys. Chem. B* **2003**, *107*, 2788.
(16) Vittadini, A.; Selloni, A.; Rotzinger, F. P.; Grätzel, M. *Phys. Rev. Lett.* **1998**, *81*, 2954.
(17) Tilocca, A.; Selloni, A. *J. Chem. Phys.* **2003**, *119*, 7445.
(18) Car, R.; Parrinello, M. *Phys. Rev. Lett.* **1985**, *55*, 2471.
(19) We used the Car-Parrinello code developed by Pasquarello, A., Laasonen, K., Trave, A., Car, R., Giannozzi, P. and others. An initial public release can be downloaded at www.democritos.it/download/sw.
(20) Perdew, J. P.; Burke, K.; Ernzerhof, M. *Phys. Rev. Lett.* **1996**, *77*, 3865.
(21) Vanderbilt, D. *Phys. Rev. B* **1990**, *41*, 7892.
(22) Burdett, J. K.; Hughbanks, T.; Miller, G. J.; Richardson, J. W., Jr.; Smith, J. V. *J. Am. Chem. Soc.* **1987**, *109*, 3639.
(23) Lazzeri, M.; Vittadini, A.; Selloni, A. *Phys. Rev. B* **2001**, *63*, 155409.
(24) Vittadini, A.; Selloni, A.; Rotzinger, F. P.; Grätzel, M. *J. Phys. Chem. B* **2000**, *104*, 1300−1306.
(25) Vittadini, A.; Selloni, A. *J. Chem. Phys.* **2002**, *117*, 353−361.
(26) Henderson, M. A.; Epling, W. S.; Perkins, C. L.; Peden, C. H. F.; Diebold, U. *J. Phys. Chem. B* **1999**, *103*, 5328−5337.
(27) Nosè, S. *Mol. Phys.* **1984**, *52*, 255.
(28) Brookes, I. M.; Muryn, C. A.; Thornton, G. *Phys. Rev. Lett.* **2001**, *87*, 266103.
(29) Henrich, V. E.; Cox, P. A. *The Surface Science of Metal Oxides*; Cambridge University Press: Cambridge, U.K., 1994.
(30) Kurtz, R. L.; Stockbauer, R.; Madey, T. E.; Román, E.; de Segovia, J. L. *Surf. Sci.* **1989**, *218*, 178.
(31) Langel, W. *Surf. Sci.* **2002**, *496*, 141−150.
(32) Two oxygens were considered to be linked by a hydrogen bond when their distance was less than 3.3 Å, the OH intermolecular distance was less than 2.4 Å, and the angle between the O−O vector and the covalent OH bond was less than 30°. These cutoff distances correspond to the first minima in the rdfs of bulk water. The same analysis applied to a classical MD trajectory of bulk SPC/E water at room temperature leads to 3.43 Hbs per molecule, with $\bar{R}_{OO}$ = 2.83 Å, $\bar{R}_{OH}$ = 1.88 Å, and an average Hb lifetime of 294 fs.
(33) Odelius, M.; Bernasconi, M.; Parrinello, M. *Phys. Rev. Lett.* **1997**, *78*, 2855−2858.
(34) Reedijk, M. F.; Arsic, J.; Hollander, F. F. A.; de Vries, S. A.; Vlieg, E. *Phys. Rev. Lett.* **2003**, *90*, 066103.
(35) Chu, Y. S.; Lister, T. E.; Cullen, W. G.; You, H.; Nagy, Z. *Phys. Rev. Lett.* **2001**, *86*, 3364.
(36) Kuhs, W. F.; Lehmann, M. S. *J. Phys. Chem.* **1983**, *87*, 4312.
(37) Redhead, P. A. *Vacuum* **1962**, *12*, 203.